JACS
JOURNAL OF THE AMERICAN CHEMICAL SOCIETY

Article

pubs.acs.org/JACS

Charge Transport across DNA-Based Three-Way Junctions

Ryan M. Young,*[,†,‡] Arunoday P. N. Singh,[†] Arun K. Thazhathveetil,[†] Vincent Y. Cho,[†] Yuqi Zhang,[§] Nicolas Renaud,[∥] Ferdinand C. Grozema,[∥] David N. Beratan,[§] Mark A. Ratner,[†] George C. Schatz,[†] Yuri A. Berlin,[†] Frederick D. Lewis,*[,†] and Michael R. Wasielewski*[,†,‡]

[†]Department of Chemistry, Northwestern University, Evanston, Illinois 60208-3113, United States

[‡]Argonne-Northwestern Solar Energy Research (ANSER) Center, Northwestern University, Evanston, Illinois 60208-3113, United States

[§]Departments of Chemistry, Biochemistry, and Physics, Duke University, Durham, North Carolina 27708, United States

[∥]DelftChemTech, Delft University of Technology, Julianalaan 136, 2628 BL Delft, The Netherlands

Supporting Information

ABSTRACT: DNA-based molecular electronics will require charges to be transported from one site within a 2D or 3D architecture to another. While this has been shown previously in linear, π-stacked DNA sequences, the dynamics and efficiency of charge transport across DNA three-way junction (3WJ) have yet to be determined. Here, we present an investigation of hole transport and trapping across a DNA-based three-way junction systems by a combination of femtosecond transient absorption spectroscopy and molecular dynamics simulations. Hole transport across the junction is proposed to be gated by conformational fluctuations in the ground state which bring the transiently populated hole carrier nucleobases into better aligned geometries on the nanosecond time scale, thus modulating the $\pi-\pi$ electronic coupling along the base pair sequence.

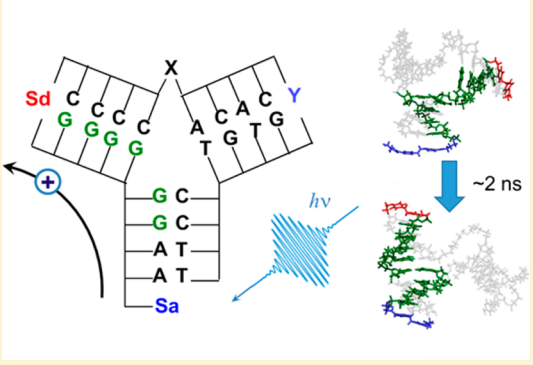

INTRODUCTION

Charge transport across a junction is a necessary condition for the construction of a molecular switch or higher circuit element. While long-range charge transport, and even wire-like behavior has been observed in duplex DNA,[1,2] at present it is unclear whether transport across a junction is favorable or practical in a DNA-based system.[3−5] Hole transport through linear poly(purine) DNA sequences has been shown to be more efficient than along random or alternating base pair sequences,[6−8] and so the flow of charge in a DNA-based assembly can be preferentially guided by rational design. The rate of hole transport through π-stacked base pair sequences has been shown to depend on the distance between the donor and the terminal acceptor, and several explicit candidate mechanisms have been proposed.[7,9−11] Charge transfer over 2−3 base pairs is generally accepted to occur via a coherent superexchange or tunneling mechanism with an exponential rate dependence on distance,[12,13] while for longer sequences, transfer is generally believed to occur by incoherent hopping with a power-law distance dependence.[6,14,15] Recently, a new mechanism was proposed for the intermediate regime where the hole can be delocalized across the entire purine tract, which reduces to coherent tunneling and to incoherent hopping at appropriate length scales.[11] Dynamical structural effects have also been considered,[16−21] with fluctuations creating a "flickering resonance" between electronic states on adjacent base pairs, which gates the charge transfer.[22] In DNA-based junctions, the situation is more complex compared to linear hairpin systems due to the local structure and conformational flexibility at the junction site, which could either impede or promote charge transfer across the junction, leading to a multiplicity of mechanisms at play.[23−26]

Charge transport across DNA four-way junctions (4WJ) and three-way junctions (3WJ) was investigated by means of photoinduced oxidation resulting in strand cleavage at guanine over a decade ago.[5,27,28] For example, Sen and co-workers found that oxidative cleavage in a 4WJ possessing an anthraquinone (AQ) oxidant covalently attached to one of its two helical stacks (Figure 1a) undergoes strand cleavage only in that stack and not in the stack attached via the 4WJ.[4] Schuster subsequently investigated hole transport in 3WJs having tethered or intercalated appended AQ oxidants and found that cleavage occurred in all three arms of structures having base pairing at the junction and a single strand TT loop at the junction (Figure 1b,c), albeit in substantially reduced efficiency when compared to cleavage in duplex structures having similar base sequences.[5] Lee has attributed quenching of the fluorescence of the dye fluorescein by AQ and rhodamine, when the three chromophores are attached to the ends of a

Received: January 27, 2015
Published: March 30, 2015

DOI: 10.1021/jacs.5b00931
J. Am. Chem. Soc. 2015, 137, 5113−5122

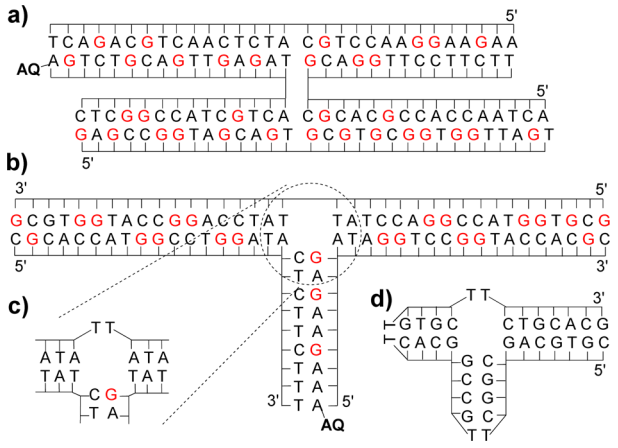

Figure 1. Structures of (a) an anthraquinone (AQ)-tethered four-way junction (after Fahlman et al.[4]), (b and c) AQ-tethered three-way junctions with and without a TT loop at the junction (after Santhosh and Schuster[5]) and (d) a compact single strand three-way junction (after Muhuri et al.[30]).

DNA-Zn^{2+} complex to electron transfer via a 3WJ in a M-DNA complex.[29]

We report here the results of a collaborative investigation of synthesis, structure, and photoinduced hole transfer across molecular 3WJs in the DNA conjugates **1**–**6** shown in Figure 2. These structures are similar in general design to the 3WJs employed by Sugimoto in investigating the effects of crowding on the stability of 3WJs (Figure 1d).[30] Our 3WJs are synthesized as single strand DNA conjugates possessing a stilbenediether (Sd) electron donor and a hexaethylene glycol (PEG) serving as linkers connecting two of three arms of the 3WJ and a stilbenediamide (Sa) electron acceptor serving as a capping group for the third arm. Conjugates **1**–**4** possess a second PEG linker at the junction site, whereas conjugates **5** and **6** possess a TT loop at this position. Conjugates **1**, **3**, and **5** possess A_2G_6 poly(purine) base sequence separating Sa and Sd, analogous to that in duplex **7** and employed in our previous studies of hole transport in diblock purine duplexes.[8] Conjugates **2**–**6** have a G–G mismatch analogous to that in duplex **8** located prior to the 3WJ. Molecular mechanics simulations are employed to evaluate the potential pathways for hole transport in these 3WJs. Finally, the dynamics and efficiency of hole transport from Sa to Sd across the 3WJ in **1**–**6** are determined by means of femtosecond time-resolved transient absorption spectroscopy. The time-dependent behavior of the Sd trap site populations suggests that arrival is ultimately limited by a stochastic process, such as a transient structural fluctuation wherein the purine bases near the junction are brought into close alignment, effectively gating the crossing event. Molecular dynamics simulations are presented to support this mechanism.

RESULTS AND DISCUSSION

Design Considerations. Photoinduced electron transfer from a stilbenediamide electron acceptor to a stilbenediether electron donor was selected as the model system for establishing the occurrence of charge transport across a 3WJ. We have previously studied the dynamics and efficiency of hole transport in Sa–Sd capped hairpins by means of femtosecond transient absorption spectroscopy.[8,31] The highest quantum yields for charge separation capped hairpins that we have observed are ca. 25% for diblock purine sequences (e.g., A_2G_n and A_3G_n, n = 6–19).[8,14] The diblock systems take advantage of the dynamics of hole transport in G-tracts, which are the fastest that have been measured for a naturally occurring base. Quantum yields for short capped hairpins (fewer than 6 base pairs) poly(purine) and alternating base sequences are too low to measure (<3%) using our methodology.[8] Santosh and Schuster have estimated that the yield of strand cleavage resulting from hole transport across their 3WJ (Figure 1b) is at least an order of magnitude lower than in an analogous duplex system.[5] Since a decrease in efficiency from 25% to <3% would make it impossible to detect the occurrence of hole transport across a 3WJ, G-tracts were selected to move the charge across the junction in systems **1**–**6**.

The 3WJs **1**–**6** all possess a Sd linker and Sa capping group at the ends of two of their three arms and a PEG linker at the

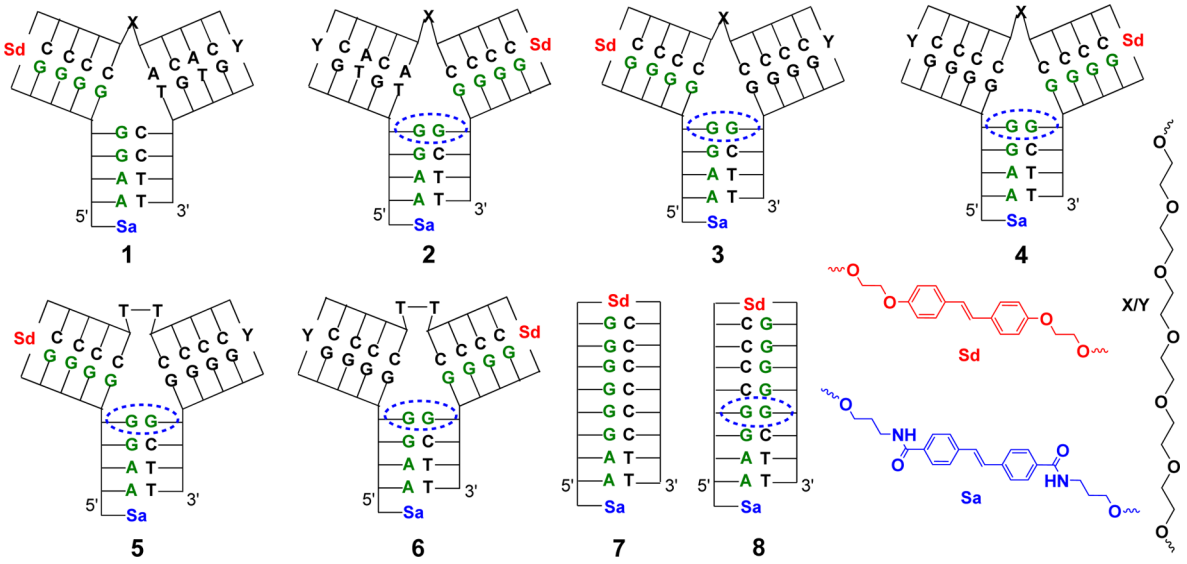

Figure 2. Structures of three-way junctions **1**–**6**, hairpins **7** and **8**, linkers Sd, X = Y, and the capping group Sa. G–G mismatches in **2**–**6** and **8** are enclosed by dotted ovals.

DOI: 10.1021/jacs.5b00931
J. Am. Chem. Soc. 2015, 137, 5113–5122

end of the third arm (Figure 2). The Sd and PEG linkers have previously been employed in the synthesis of stable mini-hairpins[32,33] and the Sa capping group in the synthesis of stable capped hairpins.[34] The 3WJs **5** and **6** possess a TT loop at the junction opposite the arm possessing the Sa capping group. The TT loop is introduced to relieve the strain present in fully base-paired junctions and to increase their flexibility. The synthetic PEG linker is substituted for the TT loop in 3WJ's **1**−**4** in order to avoid the possible disruption of poly(purine) hole transport pathways by insertion of the extra thymine bases. The 3WJ's are synthesized as a single strand containing hairpin linkers, TT or PEG junction loops, and capping group. The use of three separate end-labeled strands for the construction of 3WJs would require much longer strands to achieve stable base pairing.[29] We have avoided the use of small molecules[35] and Mg^{2+} ions[30] to stabilize the 3WJ, wishing to focus initially on hole transport across flexible, unmodified junctions.

The 3WJs **1**, **3**, and **5** have a A_2G_6 diblock purine sequence between Sa and Sd, as does capped hairpin **7**. The use of hairpin linkers and capping groups and multiple G-C base pairs is designed both to stabilize the relatively short arms of the 3WJs and to provide moderately efficient pathways for hole transport. The introduction of a G−G mismatch in the arm possessing the Sa capping group of **2**−**6** is intended to facilitate charge splitting between the two arms separated from Sa by the 3WJ. To our knowledge, hole transport across a G−G mismatch has not been investigated; however, hole transport across one or more A−A mismatches is more efficient than across other mismatched base pairs.[36,37] G−G mismatches are known to adopt a number of hydrogen-bonded geometries as well as an unusual interdigitated (zipper-like) stacking motif.[38] If rapid equilibration of the hole between the two G's occurs prior to junction crossing, then the hole could either remain in the A_2G_6 sequence of **1**, **3**, and **5** or cross over to the Sd-linked G-tract of **2**, **4**, and **6**. Capped hairpin **8** serves as a model for investigation of the efficiency and dynamics of hole transport in A_2G_6 sequence containing a G−G mismatch. The location of the G−G mismatch at the entrance to the junction of **3**−**6** is essential in order to split the change between the two G-tract arms.

Synthesis and Characterization of the Three-Way Junctions. The synthesis and characterization 3WJs and hairpins in Figure 2 are described in Supporting Information. Following synthesis and purification, the 3WJs and hairpins are characterized by their MALDI mass spectra, UV and Circular Dichroism (CD) spectra, and thermal dissociation profiles (see Supporting Information). UV absorption spectra (Supporting Information Figure S6a) display bands in the 300−350 nm region assigned to overlapping absorption of the Sa and Sd chromophores and stronger bands with maxima <300 nm characteristic of base pair absorption. The CD spectra of the 3WJs and hairpins display minima and maxima near 240 and 260 nm, respectively, with the band intensities dependent on the base sequence (Supporting Information Figure S6b). The CD spectra are similar to those of mini-hairpins having Sd or PEG linkers and G-C stems and thus presumably are dominated by the arms of the 3WJ with the strongest base pairing.[39] These Sd-linked mini-hairpins have B-DNA structures in aqueous solution.[39] Weak bands are observed in the >300 nm region of the CD spectra and are assigned to exciton coupling between the Sa and Sd chromophores. These bands are of similar or lower intensity compared to hairpins of the same sequence length, confirming that the arms of the 3WJs do not fold back on themselves to bring the chromophores into close contact.[31]

Thermal dissociation profiles for the 260 nm absorption bands of **1**−**8** are shown in Supporting Information Figure S5. The profiles for hairpins **7** and **8** have first derivative peaks >80 °C, similar to those for related Sa−Sd capped hairpins.[31] The lower onset of melting for **8** vs **7** is consistent with the presence of a G−G mismatch in the latter but not the former hairpin. The broad thermal dissociation profiles for 3WJs **1** and **2** have first derivatives, which provide values of T_M = 48 and 44 °C, respectively, substantially lower than those of hairpins **8** and **7**. Plausibly, these transitions correspond to melting of the less stable PEG-linked and/or Sa-capped arms of the 3WJ which have both A−T and G−C base pairs, with dissociation of the Sd-linked arm occurring at higher temperatures.[39] A Sd-linked mini-hairpin with only 3 G−C base pairs has a reported T_M > 80 °C. The 3WJs **3**−**6** display a continuous increase in UV intensity from 10 to 90 °C with a low degree of hyperchromism. Hyperchromism may result from premelting of the Sa-capped arm with melting of the two poly(G) arms occurring above 80 °C. Independent melting of the three arms is consistent with the structures obtained from molecular dynamics simulations (see below).

Molecular Dynamics Simulations. Information about the potential structures available to the 3WJs and hairpins was obtained by means of molecular dynamics simulations. The methods employed are described in Supporting Information. Simulated structures for 3WJs **1**−**4** hairpins **7** and **8** obtained after 12 ns simulation time are shown in Figure 3a. The poly(purine) pathways between Sa and Sd are highlighted in these structures. The structure for hairpin **7** has a B-DNA geometry for the base pairs and is similar to that previously reported for a hairpin with 8 A−T base pairs separating a Sa linker and Sa capping group.[40] The G−G mismatch both in 3WJ **2**−**4** and in hairpin **8** adopts a zipper-like stacked conformation rather than a hydrogen-bonded conformation. This may prove advantageous for hole transport as it allows for hole transport via a stacked purine array rather than across a hydrogen-bonded interface.[41] The continuous array of purine bases between Sa and Sd is severely disrupted at the 3WJ in **1** and **2**. This suggests that either hole transport occurs via alternative pathways or via minor conformations having better stacking of purine bases across the 3WJ. The latter possibility is illustrated in Figure 3b in the case of 3WJ **2**. Switching of the Y to T geometry of the 3WJ, observed in the simulations to occur within a few nanoseconds (Supporting Information Figures S26 and S27), results in improved base pair stacking between Sa and Sd but requires hole transport via a hydrogen-bonded G−G mismatch.

The structures obtained from of MD simulations for **1**−**4** are similar to those from previous studies of the solution structures of 3WJs using AFM and X-ray scattering with molecular simulation.[42,43] These studies show that the junctions are highly dynamic and have a broad distribution of angles between arms, including T and Y shaped structures. However, the angles between arms are smaller than those expected for planar symmetrical junctions. Recently, the structure of a fully complementary 3WJ having an expanded branch point has been reported based on high resolution single molecule FRET and molecular modeling.[44] Unpairing of the bases adjacent to the junction permits formation of a large cavity at the junction center. The presence of flexible TT or PEG linking elements at

DOI: 10.1021/jacs.5b00931
J. Am. Chem. Soc. 2015, 137, 5113−5122

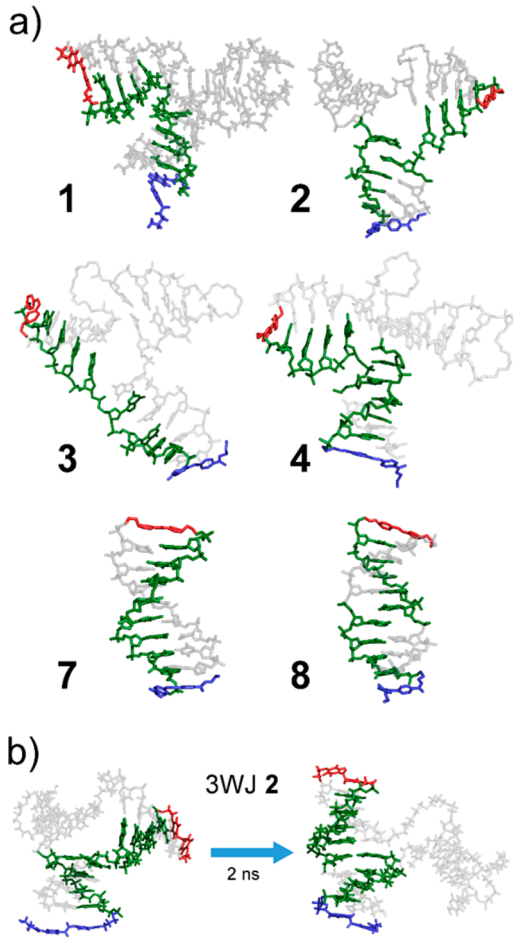

Figure 3. (a) Molecular Dynamics simulations of DNA structures **1**−**4** and **7** and **8** at 12 ns of simulation time. (b) Molecular Dynamics trajectory of 3WJ **2** showing interconversion between Y- and T-shaped structures within 2 ns.

our junctions is intended to minimize unpairing of bases adjacent to the junction.

Femtosecond Transient Absorption Spectroscopy. Hole migration dynamics in the DNA systems shown in Figure 2 were launched and probed using femtosecond transient absorption spectroscopy at room temperature. Details of our transient absorption apparatus are given in the Supporting Information. For both 3WJ and hairpin architectures the Sa moiety is selectively excited with a 100 fs, 350 nm pulse and ensuing dynamics are monitored over the following 7 ns using a broadband continuum probe.[45] Representative spectra are shown in Figure 4 and Supporting Information Figure S7. The local singlet excited state ^{1}Sa* absorption is centered at 575 nm and is initially broad, then decays as the hole is injected into the adjacent purine diblock.[7,46] The shoulder near 530 nm becomes more pronounced and distinct at later times and is assigned to absorption by the $Sd^{\bullet+}$ radical cation.[7,47] Figure 4 shows that the transient absorption spectra for 3WJ **1** and the A_2G_6 hairpin **7** exhibit similar spectral features and temporal evolution, specifically the growth of the $Sd^{\bullet+}$ absorption at long delays, though with lower intensity in the 3WJ **1**. Similar results are seen for all 3WJs presented here. The presence of the $Sd^{\bullet+}$ signal importantly demonstrates that charges can indeed transit the junction and migrate beyond the junction to a trap 20−25 Å away, while the incomplete decay of both bands suggests that

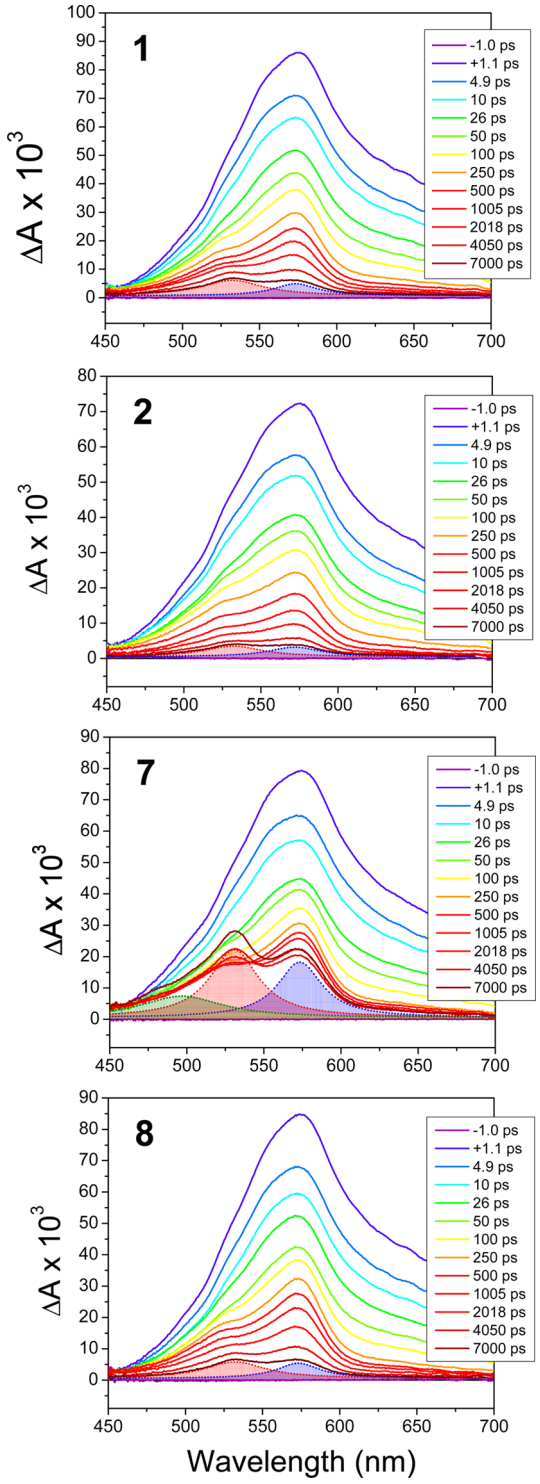

Figure 4. Femtosecond transient absorption spectra of DNA 3WJs **1** and **2** and hairpins **7** and **8** from a representative data set. Following ~100 fs, 350 nm selective excitation, Sa is locally excited to produce the maximum at 575 nm (^{1}Sa*). Oxidation of Sd is tracked by increase of the band at 530 nm. Lorentzian fits for $Sa^{\bullet-}$ (blue) and $Sd^{\bullet+}$ (red) centered near 530 and 575 nm, respectively, are shown for Δt = 7000 ps.

some of the amplitude of this signal at 575 nm is due to absorption from states where the hole has yet to reach the trap, i.e., $Sa^{\bullet-}-(A_2G_n)^{\bullet+}$,[48] with amplitude near 575 nm but not 530 nm. It is worth noting that the oxidation of Sd shows

DOI: 10.1021/jacs.5b00931
J. Am. Chem. Soc. 2015, 137, 5113−5122

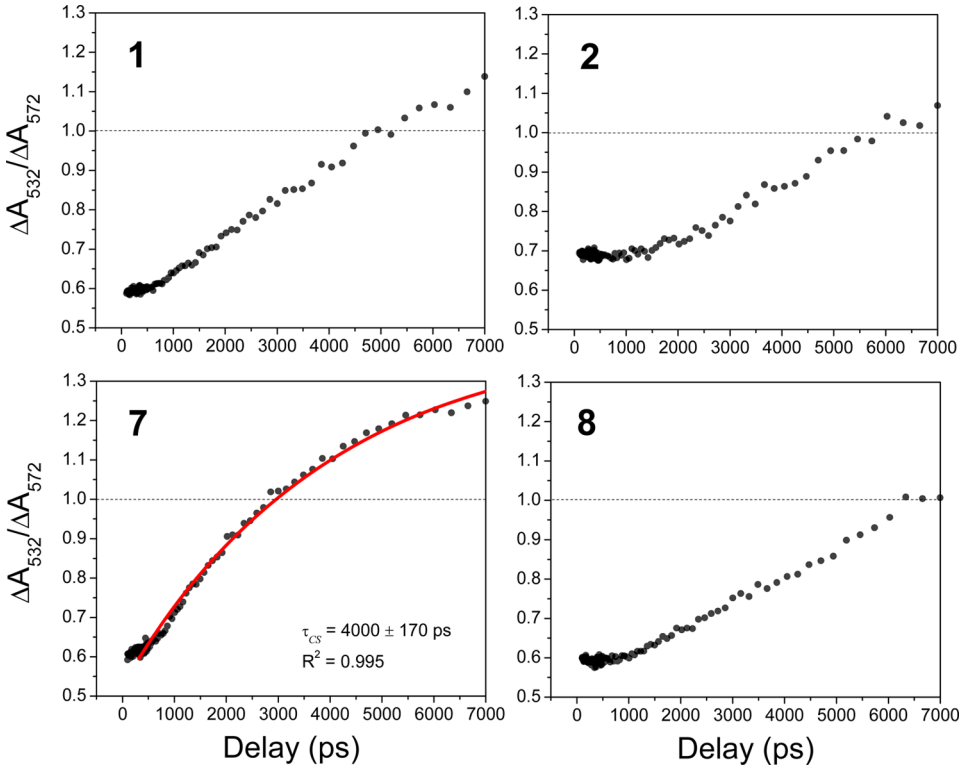

Figure 5. Ratio of $Sd^{\bullet+}$ and $Sa^{\bullet-}$ absorptions at 532 and 572 nm for 3WJs **1** and **2**, and hairpins **7** and **8** for a representative data set. Exponential fit is shown as solid red line. Data from the first 50 ps are suppressed for clarity.

definitively that the junction does not itself serve as a local hole trap preventing hole transit.

While junction crossing and subsequent trapping are demonstrated above in 3WJ **1** possessing a single direct route (G-tract) to the hole acceptor, for DNA-based systems like these to properly serve as molecular junctions in device applications, the hole must be able to migrate to either terminus. To that end, we have examined the hole transport dynamics in 3WJ **2**–**6** and control hairpin **8**, each with a G–G mismatch at the second G and a G_5-tract on the opposing strand. Hole migration is favored along G-tracts,[8] so after arriving at the mismatch, the hole is expected to propagate toward the acceptor in the hairpin and across the junction in the 3WJ; in both cases the hole must still hop between strands in order to stay along the path with the highest electronic coupling. This may be aided by the zipper-like motif observed for these structures in the MD simulations (Figure 3). In 3WJs **2**–**6** and hairpin **8**, the 530 nm band again appears at long delays indicating hole trapping by the Sd acceptor. The intensity of the 530 nm bands relative to the 575 nm bands for **2** is lower than that for the direct case **1** presumably due to the inefficient strand hopping process prior to crossing the junction. Importantly, the relative amplitude of the $Sd^{\bullet+}$ absorption band in hairpin **8** is similar to that of 3WJ **1** at long times, strongly suggesting that the rates of junction crossing and strand hopping are similar. The reduced rates of junction crossing and strand hopping expose more of the hole population to competing decay pathways, such as strand cleavage, leading to decreasing overall signals and limited yields than in comparable hairpin systems. However, we have previously observed in those diblock hairpin systems that once the hole trapping is complete, the ratio becomes constant in time because the $Sa^{\bullet-}$ and $Sd^{\bullet+}$ absorption bands exhibit the same time evolution, and the charge can reside on Sd for tens to hundreds of nanoseconds.[48] The similarity of the transient absorption spectra of **5** and **6** to those of **1**–**4** at 7 ns strongly indicates that replacing the PEG linker with a natural base TT loop does not dramatically affect either the dynamics or the terminal yields of the Sd.

Kinetics of Junction Crossing. Unambiguously quantifying the yields and rates of charge transfer is challenging owing to the broad, overlapping absorption bands of the ionic states of the stilbene moieties.[46,49] Previously, we have shown that the hole arrival times can be estimated from the exponential rise of the ΔA ratio between the $Sa^{\bullet-}$ and $Sd^{\bullet+}$ transient absorption bands.[7,50] Band ratios are shown in Figure 5. In all cases, the ratios increase over time, definitively showing that the absorption at 530 nm is from an independent source despite the overall decrease in signal intensity. Fitting the ratio for hairpin **7** shows that hole arrival occurs in 4000 ± 200 ps, in excellent agreement with the previously published value (4200 ± 400 ps).[8] However, as shown in Figure 5, for the other DNA systems studied here the ratios are generally nonexponential in time, and may actually appear linear, making exponential fitting unreliable. Since the ratios never become constant (except for **6**, see below), we conclude that hole trapping is incomplete within the 7 ns experimental time window. Hole transport therefore must be substantially slower in these systems than in hairpins of the same length and base pair sequence, implying that junction crossing is the rate-limiting step for **1**. In hairpin **8**, in which there is the G–G mismatch, hole transport is substantially slower than in control hairpin **7**. As seen in the MD simulations (Figure 3), the G–G mismatch is actually unpaired in a slipped arrangement that varies over time, which disrupts π–π stacking of the G-tract on the 5′ strand, so that the slow trapping dynamics reflect this disruption. Accordingly

DOI: 10.1021/jacs.5b00931
J. Am. Chem. Soc. 2015, 137, 5113–5122

for linear hairpin **8**, the ΔA ratio between the $Sa^{\bullet-}$ and $Sd^{\bullet+}$ transient absorption bands at early times is nearly constant before slowly increasing (Figure 5), suggestive of an induction period prior to hole migration,[8] possibly due to shuffling of the G−G pair that is reliant on thermal or solvent fluctuations.

The G−G mismatch is also present in 3WJs **2**−**6**. Sequences **3** and **5** with a direct poly(purine) path to the junction and then to the acceptor appear to demonstrate first-order rises of their band ratios, with similar arrival times to hairpin **7**, though with substantially reduced yields. However, in **2**, **4** and **6** with this mismatch and a G-tract pathway that requires the hole to cross strands prior to crossing the junction, the kinetics appear to deviate substantially from first-order behavior. Interdigitation of the guanines leads to poor $\pi-\pi$ stacking and electronic coupling, resulting in a similar induction period observed in the band ratios. The structural fluctuations leading to the Y → T interconversion are also observed in the MD simulations to disrupt the interdigitation, plausibly linking the kinetic behaviors observed in hairpin **8** and the 3WJs. Importantly, 3WJ **1** does not possess a G−G mismatch but still displays a *linear* growth of the band ratio with time, indicating that the fluctuations and slow hole transport are not solely a function of the G−G mismatch, but are also connected to the larger sequence conformation and associated dynamics. We interpret the difference between the direct (**3** and **5**) and indirect path (**2**, **4**, and **6**) behaviors to a higher population of T-form ground state conformations prior to excitation, where they would behave more similarly to B-form DNA hairpins, though still capable of converting conformations. The propensity for the T-conformation is likely due to the presence of an additional extended G-tract enhancing the stacking, which is supported by both the CD spectra and the thermal dissociation profiles indicating stronger stacking and higher melting points, respectively, for **3**−**6**. In the T-conformation, the G−G mismatch would then dominate the kinetics of the system.

The linear behavior of the band ratio for 3WJs **1**, **2** and **4** is reminiscent of pseudozero order kinetics, where the transport event is limited by a stochastic process. This is discussed in detail below. Alternatively, if the hole migration in 3WJs is governed by the same mechanism as in the hairpins, then the rate of junction crossing may be so low so as to make the ratio simply appear linear on this time scale. Modeling the hole trapping processes in these 3WJs using various sequential first-order models did not adequately capture the rise of the $Sd^{\bullet+}$ absorption band. On the basis of the approximately linear behavior observed in the band ratios, the trapping step was instead modeled using zero-order rate process with the other hole transport pathways remaining first-order; this model is shown schematically in Figure 6. $\Delta A(t)$ at selected wavelengths spanning the spectral range are globally fit to the solution to this kinetic model. With the use of these fits, the total data set is deconvoluted to give the spectra associated with each species in the model. A representative fit for 3WJ **1** is shown in Figure 7a, with the kinetic solution and associated spectral deconvolution shown in Figure 7, panels b and c, respectively. As can be seen, the data and model are in good agreement, and the spectrum associated with the zero-order growth agrees well with the absorption spectrum of $Sd^{\bullet+}$, peaking at 530 nm.[49]

In light of the Y → T conversion observed in the MD simulations for all 3WJs, the same model was used to analyze all 3WJ sequences in Figure 2, with similar agreement (Supporting Information Figures S10−S17), suggesting that this mechanism is at play to some degree in all 3WJs studied here. Results from

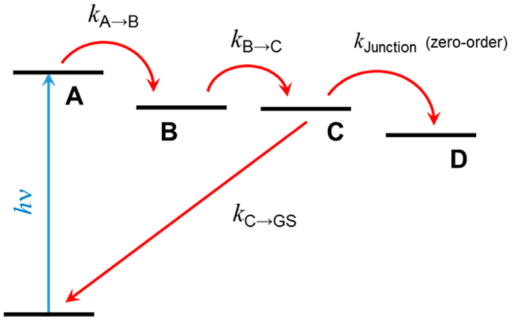

Figure 6. Simplified kinetic scheme for hole transport in the DNA 3WJs presented here. Local excitation of Sa (species A) is followed by first-order formation of a contact ion pair $Sa^{\bullet-}$−$A^{\bullet+}$ (species B). The hole then moves further along the poly(purine) sequence (first-order formation of species C) until it reaches the junction. Formation of the trapped charge-separated state $Sa^{-\bullet}Sd^{+\bullet}$ is rate-limited by junction crossing (zero-order, species D).

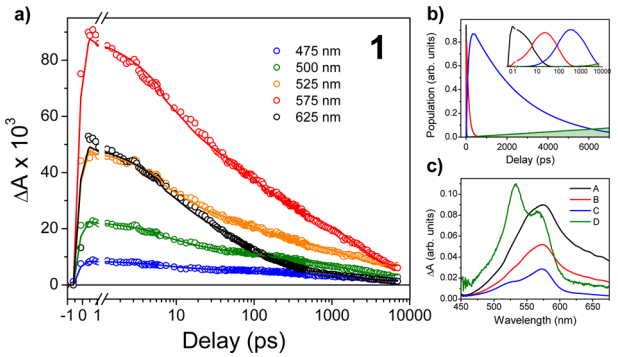

Figure 7. (a) Global fits to selected wavelengths in 3WJ **1** to the kinetic model described in the text. Fitted time constants are listed in Table 1. Fits are shown as solid lines. (b) Solution to the kinetic model using the fit parameters, with semi-log scale in inset. The pseudo-zero order population is shaded (D, green). (c) Species-associated spectra obtained from deconvolution of the data set with the kinetic fit solution. The relative intensity of the zero-order species (D, green) is arbitrary.

the fits to the kinetic model are given in Table 1. Within statistical uncertainties, the time scales of contact ion pair formation ($\tau_A \to {}_B = 1/k_{A\to B}$), hole migration ($\tau_B \to {}_C = 1/k_{B\to C}$), and charge recombination ($\tau_C \to {}_{GS} = 1/k_{C\to GS}$) are all similar for **1**−**6**, as expected since they share the same basic base pair sequence. Importantly, the zero-order rates, $k_{Junction}$, are also statistically similar, indicating that the process is insensitive to the nature of the linker (PEG or TT) and the local nucleobase pair (G−C or G−G) at the junction. The rise times from single exponential fits to the band ratios of **3**, **5** and **7** are also given in Table 1.

We attribute the pseudo-zero order process observed in relation to the $Sd^{\bullet+}$ trap population to the structural interconversion between Y- and T-shaped geometries of the ground state observed in the MD simulations (Figure 3b), which occurs within the time window of the experiment. While zero-order rate laws are unphysical, pseudo zero-order behavior may arise when the subset of molecules able to react is small (e.g., chemical conversion in a saturated enzyme) or limited by a factor external to the molecule acting as a bottleneck.[51] Here, due to the large disruption of $\pi-\pi$ stacking in the Y-geometry, hole transport is likely inefficient. Conversely, by adopting a T-shape, the base pairs are better able to stack and the electronic

DOI: 10.1021/jacs.5b00931
J. Am. Chem. Soc. 2015, 137, 5113−5122

Table 1. Summary of Quantum Yields of Hole Trapping and Kinetic Parameters for DNA Systems Studied Here[a]

sample	Φ_{trap}	τ_{ratio} (ps)	$\tau_{A\rightarrow B}$ (ps)	$\tau_{B\rightarrow C}$ (ps)	$\tau_{C\rightarrow GS}$ (ps)	$\tau_{C\rightarrow D}$ (ps)	$k_{Junction}$ ($10^{-6} \times \Delta A$ ps^{-1})
1	0.064 ± 0.010	-	7.6 ± 2.0	96 ± 12	2040 ± 448	-	9.9 ± 0.2
2	0.045 ± 0.008	-	4.2 ± 0.6	84 ± 6	1670 ± 46	-	9.5 ± 0.1
3	0.070 ± 0.020	4100 ± 200	7.1 ± 0.5	107 ± 13	2240 ± 200	-	9.1 ± 0.6
4	0.065 ± 0.013	-	4.6 ± 1.0	75 ± 15	1830 ± 275	-	7.9 ± 1.0
5	0.059 ± 0.018	2500 ± 70	7.7 ± 0.3	116 ± 2	2475 ± 117	-	9.5 ± 0.1
6	0.046 ± 0.010	-	5.0 ± 0.2	97 ± 7	2640 ± 145	-	8.8 ± 0.3
7	0.240 ± 0.029	4000 ± 170	9.6 ± 1.4	108 ± 19	-	3320 ± 422	-
8	0.055 ± 0.009	-	4.1 ± 0.7	60 ± 1	-	1725 ± 61	-

[a]First-order time constants of contact ion pair formation ($\tau_{A\rightarrow B} = 1/k_{A\rightarrow B}$), hole migration ($\tau_{B\rightarrow C} = 1/k_{B\rightarrow C}$), and charge recombination ($\tau_{C\rightarrow GS} = 1/k_{C\rightarrow GS}$). Hole trapping in linear hairpins is modeled by a first-order process ($\tau_{C\rightarrow D} = 1/k_{C\rightarrow D}$), while in 3WJs it is assumed to be rate-limited by conformational gating and modeled using a zero-order rate ($k_{Junction}$). Values and uncertainties are reported as averages and standard errors of the mean, respectively, over multiple experiments.

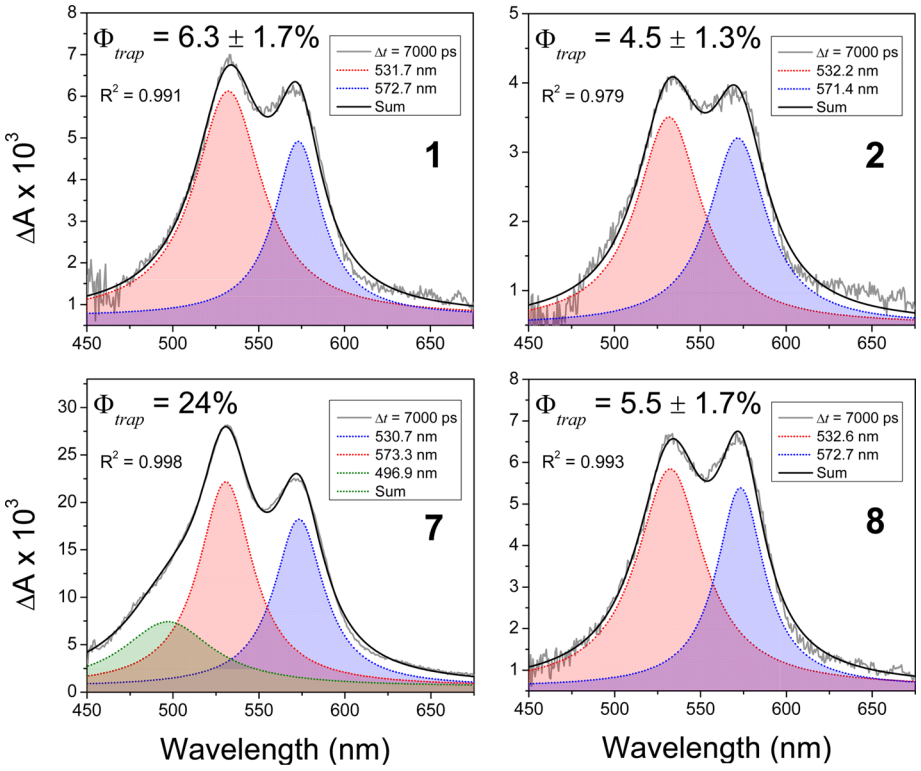

Figure 8. Lorentzian fits at Δt = 7000 ps for selected DNA structures for a representative data set (gray). The 530 nm band (red) and 575 nm band (blue) are shaded, and the sum of the two fits is shown as the solid black line. Hairpin **7** shows a short-wavelength absorption shoulder (green) associated with $Sd^{+\bullet}$ that is only observable at high yields.

coupling will subsequently be higher, similar to the cases of guanine tracts in B-form DNA; these conformations will more readily support hole transport. Because the structures studied here can interconvert within a few nanoseconds, at which time there is still hole population within the G-tract at the junction, the interconversion serves as a conformational gating mechanism.[52,53] The induction period observed in the band ratio kinetics is plausibly a consequence of the hole "waiting" for the interconversion event prior to crossing the junction and trapping by Sd. That $k_{Junction}$ is the same for **1**−**6** is consistent with this mechanism. The necessary condition that the rate of charge recombination from holes localized before the junction must be lower than or competitive with that of interconversion in order for junction crossing to occur appears to be satisfied: the kinetic model indicates that charge recombination from the intermediate ion pair state has a lifetime of ∼2 ns (Table 1), while the MD simulations show that the Y → T conversion is complete within that time. It should be noted that the absolute magnitudes of the zero-order rate constants are unimportant, as they are sensitive to the precise experimental conditions; however, since the experiments were all carried out under strictly similar conditions, comparisons of the relative rate constants between samples can still readily be made. No intermediate state between crossing the junction and reaching the Sd trap was observed to be necessary to fit the data, consistent with the junction crossing event being rate-determining. Recent theoretical work on linear DNA hairpins with Sa and Sd has shown that the rate-limiting step for charge transfer is hole trapping by Sd;[54] the same mechanism is likely responsible for hole trapping from the G_4-tract after the junction, however the entire trapping process would likely still be gated by structural interconversion.

Hole Trapping Yields. Because the hole arrival process is not complete within 7 ns, we can only approximate the

DOI: 10.1021/jacs.5b00931
J. Am. Chem. Soc. 2015, 137, 5113−5122

quantum yields of hole trapping by the acceptor. Incomplete hole transfer implies the presence of $Sa^{\bullet-}$ absorption that does not result from a $Sa^{\bullet-}/Sd^{\bullet+}$ pair; photogenerated $Sa^{\bullet-}$ can decay through multiple pathways prior to the hole crossing the junction and subsequent oxidation of Sd, and so the contributions to the spectra from each radical ion will evolve independently. The zero-order nature of the gating process makes comparisons of the relative intensities of the reconstructed species-associated spectra very challenging. To better account for the two radical ion populations separately, the transient absorption spectra at 7 ns were deconvolved into Lorentzian profiles from $Sa^{\bullet-}$ and $Sd^{\bullet+}$ near 575 and 530 nm, respectively. After the initial hole injection from $^1Sa^*$ to the adjacent purine sequence, the transient spectra will mostly resemble the absorption spectrum of $Sa^{\bullet-}$, as the purine base cations have been shown to have very low extinction coefficients.[55−57] While $^1Sa^*$ absorbs in the 575 nm region, the excited state lifetime of $^1Sa^*$ is only ∼220 ps,[46] so changes in the signal at times significantly longer than this must be due to a different chemical species. Accordingly, quantum yields for charge separation, Φ_{trap}, are approximated using eq 1,

$$\Phi_{trap}^{TWJ} = \left(\frac{\Delta A_{Sd^{\bullet+}}}{\Delta A_{Sa^*}}\right)_{TWJ} \div \left(\frac{\Delta A_{Sd^{\bullet+}}}{\Delta A_{Sa^*}}\right)_{Hairpin} \times \Phi_{CS}^{Hairpin} \quad (1)$$

where ΔA_{Sa^*} is the amplitude of the transient absorption spectrum at Δt = 500 fs, and $\Delta A_{Sd^{\bullet+}}$ is the amplitude plus offset of the Lorentzian fit near 530 nm at Δt = 7000 ps—the maximum delay of the experiment. The yield Φ_{trap} is determined relative to hairpin **7** (reported previously as 24%[8]) as it has the same base pair sequence. In this way, the band intensity ratio intrinsically accounts for variations in experimental parameters such as concentration, pump−probe overlap, and laser fluence. Lorentzian decompositions at Δt = 7 ns and associated quantum yields are shown in Figure 8, and a detailed description of the fitting procedure is given in the Supporting Information. Quantum yields of hole trapping for the 3WJs studied here are all ∼4−7%, and are summarized in Table 1.

The similarity and the magnitudes of the quantum yields in the 3WJs relative to the hairpins having the same base pair sequence again indicate that traversing the junction is the rate-limiting step for the direct path systems. This is consistent with the stochastic Y ↔ T structural interconversion discussed above serving as a global gating mechanism for hole transport. Variations in yield observed here may consequently reflect details in the structures of the T-conformers and their modulations of the G−G electronic coupling. The similar trapping yields observed for the PEG- and TT-linked 3WJs also support this, since hole transport is favored in the T-conformation, the nature of the linker should only have a minor effect.

The loss of G−G coupling due to interdigitation is apparent in **8** as well: the yield Φ_{trap} is only ∼1/4 of that for hairpin **7**, since the base pairing disruption also reduces the π-overlap and thus the rate of hole transfer. Interestingly, the ∼5% yield for **8** is similar to that observed for the direct-route 3WJ **1** (∼6%). This strongly suggests that efficiency of crossing the junction (via gating) is comparable to that of interstrand hopping despite the different conformations and resulting orbital overlaps.

From the both the similarity of yields and the steady-state spectroscopy, it appears that 3WJs **3** and **4** possess slightly different structures than **1** and **2** imposed by the third G tract. Comparison of the 532 nm/572 nm band ratios for the systems studied here shows very similar time evolution for hairpin **7** and 3WJ **3**, while the band ratios for **8** and **4** both exhibit an apparent induction period prior to hole trapping (Figure 5 and Supporting Information Figure S8). The quantum yields for hole trapping for **3** and **4** are also comparable to that of hairpin **8** (Table 1), despite the possibility of both strand hopping and transiting the junction from the same base pair sequence. The yield for 3WJ **5** is similar to the other 3WJs, indicating the TT and PEG linkers behave similarly. Sequence **6** has the lowest yield of all the structures studied here, a feature which is also reflected in its low band ratio and anomalous kinetic behavior compared to the similar 3WJ **4**. It is possible the higher yield and band ratio in **4** are again due to the PEG linker yielding a higher fraction of T-conformers in the ground state compared to the TT linker, though there is little indication of this in the steady state spectroscopy. Whether this conformation is preferential or dynamical is unclear. The slow rate constants and low efficiencies for charge separation in the capped hairpins **7** and **8** as well as across the 3WJs may also reflect slow hole transport within the base pair domains due to the presence of the Sd linking group. To the extent that hole transport is gated by conformational fluctuations,[58] restricted conformational freedom in the Sd-linked hairpin domains could reduce the rate constants for hole transport.

Lowering the temperature should, in principle, slow the interconversion process and thereby reduce the trapping yields. Transient absorption spectroscopy at 5 °C was performed on **1**, **2**, **7** and **8** (see Supporting Information). Both the rate and yield of hole trapping were reduced in hairpin **7**, with the yield dropping to ∼12%, though the reduction in the yield may be exaggerated by the slowed rate extending the process beyond the 7 ns experimental time window. Hairpin **8** showed a substantially reduced trapping yield of approximately 1%, which is the typical statistical uncertainty for our yield measurements. Since the MD simulations show that the G−G mismatch is not well paired and more interdigitated with the base pairs on the opposite strand, it appears that hole hopping along this disrupted G-tract is thermally activated, with the barrier approximately k_BT (T = 298 K) in magnitude.

Interestingly 3WJ **1** at 5 °C shows a ∼5% yield of hole trapping by 7 ns, similar to that observed at room temperature within the statistical error of the experiments. The data for 3WJs **1** and **2** acquired at 5 °C were also fit well by the same model applied to the room temperature data, with similar values for the zero-order rate constants. This indicates that the barrier to structural interconversion $\ll k_BT$ and the reduced thermal energy may not be low enough to deactivate the necessary fluctuations and the gating pathways across the junction are still thermally accessible. Alternatively, it is possible that there is an ensemble of structures having electronic coupling between the base pairs at the junction that are favorable for junction crossing when "frozen" into place. 3WJ **2** shows almost no hole trapping, and its ΔA ratio between the $Sa^{\bullet-}$ and $Sd^{\bullet+}$ transient absorption bands is effectively flat across the entire experimental time window. The ratios for all sequences studied here exhibit slower rises at 5 °C and extended induction periods where the hole is hopping along the sequence and has yet to arrive at Sd. Due to substantially reduced yield observed for **8** at this lower temperature, we attribute the lack of trapping in **2** to a combination of the two barriers inhibiting population from reaching and ultimately

DOI: 10.1021/jacs.5b00931
J. Am. Chem. Soc. 2015, 137, 5113−5122

crossing the junction, such that no $Sd^{\bullet+}$ signal is observed and the $Sa^{\bullet-}$/purine$^{\bullet+}$ signals decay to baseline within the experimental time window.

CONCLUDING REMARKS

We have demonstrated for the first time that charge flow in DNA can be detected nondestructively in branched architectures possessing three-way junctions. The use of a G−G mismatch to equilibrate the charge entering the junction, thereby allowing it to proceed to either arm containing a hole acceptor, is also reported for the first time. The occurrence of measurable hole transport from a Sa hole donor to a Sd hole acceptor located in different arms of a 3WJ is consistent with our design considerations and with the results of molecular dynamics simulations. The yields for charge separation across the 3WJs are ca. 20−33% as large as those for the capped hairpin **7**, which possesses neither a 3WJ nor G−G mismatch. Thus, the reduction in yield is attributed, at least in part, to the combined losses for crossing the junction and the mismatch.

While the yields observed in the 3WJ designs presented here are most likely too low for effective use in molecular electronic devices, they do suggest several potential applications including switches, splitters, and combiners. Discussion of such applications should properly wait for more advanced designs which provide for more efficient transport of charge across the junction and the incorporation of longer arms separating the charge input and output. Current work in our laboratories is focused on improving the yield of hole transport and better understanding the dynamics and mechanism of the junction crossing event as well as hole transport in the hairpin base pair domains. Further studies on the temperature and viscosity dependence of the junction crossing dynamics will also give insight into the role of conformational gating.

ASSOCIATED CONTENT

Supporting Information

Synthesis and purification details, MD simulation details, HPLC chromatograms, UV absorption spectra, thermal dissociation curves, circular dichroism spectra, additional femtosecond transient absorption spectroscopy spectra and analysis. This material is available free of charge via the Internet at http://pubs.acs.org.

AUTHOR INFORMATION

Corresponding Authors

*ryan.young@northwestern.edu
*fdl@northwestern.edu
*m-wasielewski@northwestern.edu

Notes

The authors declare no competing financial interest.

ACKNOWLEDGMENTS

The authors gratefully acknowledge Dr. Stephen A. Miller for assistance with the flow cell, Scott M. Dyar for assistance with visualizing the MD simulation structures, and Dr. Matt Krzyaniak and Prof. Josh Vura-Weis for useful discussions. This research was supported by the Office of Naval Research MURI Grant No. N00014-11-1-0729 (M.R.W., F.D.L., D.N.B., Y.A.B.). R.M.Y. was supported as part of the ANSER Center, an Energy Frontier Research Center funded by the U.S. Department of Energy (DOE), Office of Science, Basic Energy Sciences (BES), under Award # DE-SC0001059.

REFERENCES

(1) *Long-Range Charge Transfer in DNA, I and II*; Schuster, G. B., Ed.; Springer: Berlin, 2004; Vol. *236−237*.
(2) Genereux, J. C.; Barton, J. K. *Chem. Rev.* **2009**, *110*, 1642.
(3) Odom, D. T.; Dill, E. A.; Barton, J. K. *Nucleic Acids Res.* **2001**, *29*, 2026.
(4) Fahlman, R. P.; Sharma, R. D.; Sen, D. *J. Am. Chem. Soc.* **2002**, *124*, 12477.
(5) Santhosh, U.; Schuster, G. B. *Nucleic Acids Res.* **2003**, *31*, 5692.
(6) Lewis, F. D.; Zhu, H.; Daublain, P.; Cohen, B.; Wasielewski, M. R. *Angew. Chem., Int. Ed.* **2006**, *45*, 7982.
(7) Lewis, F. D.; Zhu, H.; Daublain, P.; Fiebig, T.; Raytchev, M.; Wang, Q.; Shafirovich, V. *J. Am. Chem. Soc.* **2005**, *128*, 791.
(8) Vura-Weis, J.; Wasielewski, M. R.; Thazhathveetil, A. K.; Lewis, F. D. *J. Am. Chem. Soc.* **2009**, *131*, 9722.
(9) Barnett, R. N.; Cleveland, C. L.; Joy, A.; Landman, U.; Schuster, G. B. *Science* **2001**, *294*, 567.
(10) Liu, C.-S.; Hernandez, R.; Schuster, G. B. *J. Am. Chem. Soc.* **2004**, *126*, 2877.
(11) Renaud, N.; Berlin, Y. A.; Lewis, F. D.; Ratner, M. A. *J. Am. Chem. Soc.* **2013**, *135*, 3953.
(12) Lewis, F. D.; Liu, X.; Liu, J.; Miller, S. E; Hayes, R. T.; Wasielewski, M. R. *Nature* **2000**, *406*, 51.
(13) Bixon, M.; Jortner, J. In *Advances in Chemical Phyics*; John Wiley & Sons, Inc.: New York, 2007; p 35.
(14) Conron, S. M. M.; Thazhathveetil, A. K.; Wasielewski, M. R.; Burin, A. L.; Lewis, F. D. *J. Am. Chem. Soc.* **2010**, *132*, 14388.
(15) Berlin, Y. A.; Burin, A. L.; Ratner, M. A. *J. Am. Chem. Soc.* **2000**, *123*, 260.
(16) Woiczikowski, P. B.; Kubař, T.; Gutiérrez, R.; Caetano, R. A.; Cuniberti, G.; Elstner, M. *J. Chem. Phys.* **2009**, 130.
(17) Gutiérrez, R.; Caetano, R. A.; Woiczikowski, B. P.; Kubar, T.; Elstner, M.; Cuniberti, G. *Phys. Rev. Lett.* **2009**, *102*, 208102.
(18) Grozema, F. C.; Tonzani, S.; Berlin, Y. A.; Schatz, G. C.; Siebbeles, L. D. A.; Ratner, M. A. *J. Am. Chem. Soc.* **2008**, *130*, 5157.
(19) Cramer, T.; Krapf, S.; Koslowski, T. *J. Phys. Chem. C* **2007**, *111*, 8105.
(20) Berlin, Y.; Kurnikov, I.; Beratan, D.; Ratner, M.; Burin, A. In *Long-Range Charge Transfer in DNA II*; Schuster, G. B., Ed.; Springer: Berlin Heidelberg, 2004; Vol. *237*, p 1.
(21) Senthilkumar, K.; Grozema, F. C.; Guerra, C. F.; Bickelhaupt, F. M.; Lewis, F. D.; Berlin, Y. A.; Ratner, M. A.; Siebbeles, L. D. A. *J. Am. Chem. Soc.* **2005**, *127*, 14894.
(22) Zhang, Y.; Liu, C.; Balaeff, A.; Skourtis, S. S.; Beratan, D. N. *Proc. Natl. Acad. Sci. U.S.A.* **2014**, *111*, 10049.
(23) Ma, R.-I.; Kallenbach, N. R.; Sheardy, R. D.; Petrillo, M. L.; Seeman, N. C. *Nucleic Acids Res.* **1986**, *14*, 9745.
(24) Leontis, N. B.; Kwok, W.; Newman, J. S. *Nucleic Acids Res.* **1991**, *19*, 759.
(25) Duckett, D. R.; Lilley, D. M. *EMBO J.* **1990**, *9*, 1659.
(26) Leontis, N. B.; Piotto, M. E.; Hills, M. T.; Malhotra, A.; Ouporov, I. V.; Nussbaum, J. M.; Gorenstein, D. G. In *Methods in Enzymology*; Thomas, L. J., Ed.; Academic Press: New York, 1995; Vol. *261*, p 183.
(27) Genereux, J. C.; Barton, J. K. *Chem. Rev.* **2009**, *110*, 1642.
(28) Fahlman, R. P.; Sharma, R. D.; Sen, D. *J. Am. Chem. Soc.* **2002**, *124*, 12477.
(29) Wettig, S. D.; Bare, G. A.; Skinner, R. J. S.; Lee, J. S. *Nano Lett.* **2003**, *3*, 617.
(30) Muhuri, S.; Mimura, K.; Miyoshi, D.; Sugimoto, N. *J. Am. Chem. Soc.* **2009**, *131*, 9268.
(31) Lewis, F. D.; Wu, Y. S.; Zhang, L. G.; Zuo, X. B.; Hayes, R. T.; Wasielewski, M. R. *J. Am. Chem. Soc.* **2004**, *126*, 8206.
(32) Lewis, F. D.; Wu, Y. S.; Liu, X. Y. *J. Am. Chem. Soc.* **2002**, *124*, 12165.
(33) McCullagh, M.; Zhang, L.; Karaba, A. H.; Zhu, H.; Schatz, G. C.; Lewis, F. D. *J. Phys. Chem. B* **2008**, *112*, 11415.

DOI: 10.1021/jacs.5b00931
J. Am. Chem. Soc. 2015, 137, 5113−5122

(34) Zhang, L. G.; Zhu, H. H.; Sajimon, M. C.; Stutz, J. A. R.; Siegmund, K.; Richert, C.; Shafirovich, V.; Lewis, F. D. *J. Chin. Chem. Soc.* **2006**, *53*, 1501.
(35) Vuong, S.; Stefan, L.; Lejault, P.; Rousselin, Y.; Denat, F.; Monchaud, D. *Biochimie* **2012**, *94*, 442.
(36) Schlientz, N. W.; Schuster, G. B. *J. Am. Chem. Soc.* **2003**, *125*, 15732.
(37) Osakada, Y.; Kawai, K.; Fujitsuka, M.; Majima, T. *Nucleic Acids Res.* **2008**, *36*, 5562.
(38) Chou, S. H.; Chin, K. H.; Wang, A. H. J. *Nucleic Acids Res.* **2003**, *31*, 2461.
(39) Tuma, J.; Tonzani, S.; Schatz, G. C.; Karaba, A. H.; Lewis, F. D. *J. Phys. Chem. B* **2007**, *111*, 13101.
(40) Lewis, F. D.; Zhang, L. G.; Liu, X. Y.; Zuo, X. B.; Tiede, D. M.; Long, H.; Schatz, G. C. *J. Am. Chem. Soc.* **2005**, *127*, 14445.
(41) Balaeff, A.; Craig, S. L.; Beratan, D. N. *J. Phys. Chem. A* **2011**, *115*, 9377.
(42) Shlyakhtenko, L. S.; Potaman, V. N.; Sinden, R. R.; Gall, A. A.; Lyubchenko, Y. L. *Nucleic Acids Res.* **2000**, *28*, 3472.
(43) Im, K.; Jeong, D.; Hur, J.; Kim, S.-J.; Hwang, S.; Jin, K. S.; Park, N.; Kim, K. *Sci. Rep.* **2013**, 3.
(44) Sabir, T.; Toulmin, A.; Ma, L.; Jones, A. C.; McGlynn, P.; Schröder, G. F.; Magennis, S. W. *J. Am. Chem. Soc.* **2012**, *134*, 6280.
(45) Brown, K. E.; Veldkamp, B. S.; Co, D. T.; Wasielewski, M. R. *J. Phys. Chem. Lett.* **2012**, *3*, 2362.
(46) Lewis, F. D.; Wu, T.; Liu, X.; Letsinger, R. L.; Greenfield, S. R.; Miller, S. E.; Wasielewski, M. R. *J. Am. Chem. Soc.* **2000**, *122*, 2889.
(47) Lewis, F. D.; Liu, X.; Miller, S. E.; Hayes, R. T.; Wasielewski, M. R. *J. Am. Chem. Soc.* **2002**, *124*, 11280.
(48) Conron, S. M. M.; Thazhathveetil, A. K.; Wasielewski, M. R.; Burin, A. L.; Lewis, F. D. *J. Am. Chem. Soc.* **2010**, *132*, 14388.
(49) Lewis, F. D.; Liu, X.; Wu, Y.; Miller, S. E.; Wasielewski, M. R.; Letsinger, R. L.; Sanishvili, R.; Joachimiak, A.; Tereshko, V.; Egli, M. *J. Am. Chem. Soc.* **1999**, *121*, 9905.
(50) Lewis, F. D.; Zhu, H.; Daublain, P.; Cohen, B.; Wasielewski, M. R. *Angew. Chem., Int. Ed.* **2006**, *45*, 7982.
(51) Atkins, P. W.; Walters, V.; De Paula, J. *Physical Chemistry*; Macmillan Higher Education: New York, 2006.
(52) Berlin, Y. A.; Burin, A. L.; Siebbeles, L. D. A.; Ratner, M. A. *J. Phys. Chem. A* **2001**, *105*, 5666.
(53) Hoffman, B. M.; Ratner, M. A. *J. Am. Chem. Soc.* **1987**, *109*, 6237.
(54) Renaud, N.; Berlin, Y. A.; Ratner, M. A. *Proc. Natl. Acad. Sci. U.S.A.* **2013**, *110*, 14867.
(55) Lewis, F. D.; Zhu, H.; Daublain, P.; Sigmund, K.; Fiebig, T.; Raytchev, M.; Wang, Q.; Shafirovich, V. *Photochem. Photobiol. Sci.* **2008**, *7*, 534.
(56) Kobayashi, K.; Tagawa, S. *J. Am. Chem. Soc.* **2003**, *125*, 10213.
(57) Kobayashi, K.; Yamagami, R.; Tagawa, S. *J. Phys. Chem. B* **2008**, *112*, 10752.
(58) Grozema, F. C.; Tonzani, S.; Berlin, Y. A.; Schatz, G. C.; Siebbeles, L. D. A.; Ratner, M. A. *J. Am. Chem. Soc.* **2008**, *130*, 5157.

DOI: 10.1021/jacs.5b00931
J. Am. Chem. Soc. 2015, 137, 5113−5122